J|A|C|S
ARTICLES
Published on Web 05/19/2007

Stereochemical Control Mechanisms in Propylene Polymerization Mediated by C_1-Symmetric CGC Titanium Catalyst Centers

Alessandro Motta,[†] Ignazio L. Fragalà,*[,†] and Tobin J. Marks*[,‡]

Contribution from the Dipartimento di Scienze Chimiche, Università di Catania, and INSTM, UdR Catania, Viale A. Doria 6, 95125 Catania, Italy, and Department of Chemistry, Northwestern University, Evanston, Illinois 60208-3113

Received December 15, 2006; Revised Manuscript Received March 23, 2007; E-mail: lfragala@dipchi.unict.it; t-marks@nothwestern.edu

Abstract: This work analyzes stereochemical aspects of olefin polymerization processes mediated by the C_1-symmetric constrained geometry catalyst $H_2Si(ind)(^tBuN)TiCH_3^+$ (ind = indenyl), including the role of the cocatalyst/counteranion. The energetics of catalyst activation are first analyzed and shown to compare favorably with experiment. The energetics of heterolytic ion pair separation are next scrutinized, and the effects of solvation environment are assessed. Computed thermodynamic profiles for ethylene insertion at $H_2Si(ind)(^tBuN)TiCH_3^+$ indicate that the kinetics of insertion processes at the $H_2Si(ind)(^tBuN)TiR^+$ cation can be analyzed in terms of SCF potential energies. We next compare the energetic profile for ethylene insertion at the naked $H_2Si(ind)(^tBuN)TiCH_3^+$ cation with that at the related $H_2Si(ind)(^tBuN)TiCH_3^+H_3CB(C_6F_5)_3^-$ ion pair to understand counterion effects. It is seen that the counterion, although affecting overall catalytic activity, does not significantly influence enchainment stereochemistry or polymer microtacticity. Next, the second ethylene insertion at $H_2Si(ind)(^tBuN)Ti(^nC_3H_7)^+H_3CB(C_6F_5)_3^-$ is analyzed to evaluate counteranion influence on the propagation barrier. It is found that the ethylene uptake transition state is energetically comparable to the first insertion transition state and that solvation has negligible effects on the energetic profile. These findings justify analysis of the propylene insertion process within the less computationally demanding "naked cation" model. Thus, monomer enchainment at $H_2Si(ind)(^tBuN)TiR^+$ is analyzed for $H_2Si(ind)(^tBuN)TiCH_3^+$ + propylene (first insertion) and for $H_2Si(ind)(^tBuN)Ti(^iC_4H_6)^+$ + propylene (second insertion). Data describing the first insertion highlight the sterically dominated regioselection properties of the system with activation energies indicating that olefin insertion regiochemistry is predominantly 1,2 (primary), while the second insertion similarly reflects the catalyst stereoinduction properties, with steric effects introduced by the growing chain (mimicked by an isobutyl group) preferentially favoring insertion pathways that afford isotactic enrichment, in agreement with experiment.

Introduction

The past two decades have witnessed increasingly great interest in the insertive polymerization of olefins by early transition metal catalysts.[1] Group 4 constrained geometry catalysts (CGC; e.g., structure **I**) are particularly versatile and afford polyolefins with remarkable new architectures and processability characteristics.[2] Thus, a rich and varied class of catalysts is obtained by varying the metal center (group 4 elements), cyclopentadienyl substituents (H, CH_3, indenyl, fluorenyl, etc.), nitrogen substituents (CH_3, ^iPr, ^tBu, phenyl, etc.), and *ansa* linkage ($(CH_3)_2Si$, $(CH_3)_2C$, $(CH_2)_2$, etc).[2] In general, CGC systems exhibit electronic and steric properties intermediate between those of *ansa*-metallocene (e.g., $(CH_3)_2Si(R_4C_5)_2MR^+$) and half-sandwich (e.g., $(R_5C_5)MR_2^+$) catalysts.[1−4] Cyclopentadienyl-amido based CGC catalysts effect the homopolymerization of α-olefins (1-butene, 1-pentene), ethylene copolymerization with sterically encumbered comonomers, and, depending on catalyst symmetry, moderately stereoselective isotactic or syndiotactic enchainment of propylene.[2,5]

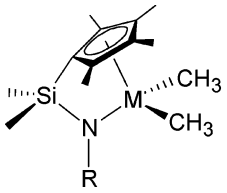

I

In this context, any detailed understanding of the experimental properties of catalytic systems must necessarily incorporate

[†] Università di Catania.
[‡] Northwestern University.

(1) For recent reviews, see: (a) Marks, T. J. ed. *Proc. Nat. Acad. Sci. U.S.A.* **2006**, *103*, 15288−15354 and contributions therein (special feature on polymerization). (b) Suzuki, N. *Top. Organomet. Chem.* **2005**, *8*, 177−216. (c) Alt, H. G. *Dalton Trans.* **2005**, *20*, 3271−3276. (d) Kaminsky, W. *J. Polym. Sci., Part A: Poly. Chem.* **2004**, *42*, 3911−3921. Wang, W.; Wang, L. *J. Polym. Mater.* **2003**, *20*, 1−8. (e) Delacroix, O.; Gladysz, J. A. *Chem. Commun.* **2003**, *6*, 665−675. (f) Kaminsky, W.; Arndt-Rosenau, M. *Applied Homogeneous Catalysis with Organometallic Compounds*, 2nd ed.; Wiley-VCH Verlag GmbH: Weinheim, Germany, 2002. (g) Lin, S.; Waymouth, R. M. *Acc. Chem. Res.* **2002**, *35*, 765−773. (h) Chen, E. Y.-X.; Marks, T. J. *Chem. Rev.* **2000**, *100*, 1391−1434. (i) Gladysz, J. A. *Chem. Rev.* **2000**, *100*, 1167−1168 and contributions therein. (j) Schweier, G.; Brintzinger, H.-H. *Macromol. Symp.* **2001**, *173* 89−103. (k) Kaminsky, W. *Catal. Today* **2000**, *62*, 23−34. (l) Kaminsky, W. *Adv. Catal.* **2001**, *46*, 89−159.

modeling studies that offer a fundamental tool for interpreting current and stimulating future experiments.[6] For processes mediated by group 4 metallocenium catalysts, quantum chemical attention has focused on mechanisms of propagation and on the effects of metal identity, cyclopentadienyl ligands,[7] counteranions, and solvation[8] on the kinetics, thermodynamics, and selectivity of the polymerization process. Computational studies of regio- and stereochemical control by group 4 catalysts have focused on metallocene and ansa-metallocene systems.[3d,9] In particular, the syndiotacticity associated with polymerization of propylene,[3d] styrene,[9a,i] and acrylates[9j] by C_s-symmetric systems and the isospecific control of propylene[9d,g] and acrylates[9j] by C_2-symmetric systems, as well as the regio- and stereoselectivity of metallocenes in the presence of heterocenes,[9k] have been extensively studied. In contrast, the stereochemical phenomenology associated with C_1-symmetric metallocene polymerization catalysts is far more complex and intricate. In fact, unlike the case for C_2- and C_s-symmetric metallocenes, studies of C_1-symmetric metallocenes evidence little direct relationship between catalyst geometry and the resulting polymer microstructure. Thus C_1-symmetric catalysts have been shown to produce polyolefins with a wide variety of microstructures ranging from atactic[10a] to syndiotactic,[10b] to hemiisotactic[10c] and isotactic[10c−e] depending on the steric and electronic environment around the metal center. These experimental results have found a convincing rationale from theoretical models adopted to highlight the principal stereochemical features of C_1-symmetric metallocene catalysts.[11] In contrast, the regio- and stereochemical features of the technologically important CGC-based catalyst systems have not been investigated theoretically. This fact motivates the present computational analysis of stereoinduction in polymerization processes mediated by a prototypical CGC Ti-based C_1-symmetric system, $(CH_3)_2Si(ind)(^tBuN)TiR^+$, which produces isotactic-enriched polypropylene.

A fundamental issue associated with stereochemical control in olefin polymerization processes is related to understanding the interrelationship between the species involved in the catalytic process. In particular, the role of the *cocatalysts/activators*, which generate highly active and stable cationic catalysts,[12−14]

(2) (a) Li, H.; Stern, C. L.; Marks, T. J. *Macromolecules* **2005**, *38*, 9015−9027. (b) Naga, N. *J. Polym. Sci., Part A: Poly. Chem.* **2005**, *43*, 1285−1291. (c) Staal, O. K. B.; Beetstra, D. J.; Jekel, A. P.; Hessen, B.; Teuben, J. H.; Stepnicka, P.; Gyepes, R.; Horacek, M.; Pinkas, J.; Mach, K. *Collect. Czech. Chem. Commun.* **2003**, *68*, 1119−1130. (d) Li, H.; Li, L.; Marks, T. J.; Liable-Sands, L.; Rheingold, A. L. *J. Am. Chem. Soc.* **2003**, *125*, 10788−10789. (e) Sinnema, P.-J.; Hessen, B.; Teuben, J. H. *Macromol. Rapid Commun.* **2000**, *21*, 562−566. (f) Altenhoff, G.; Bredeau, S.; Erker, G.; Kehr, G.; Kataeva, O.; Fröhlich, R. *Organometallics* **2002**, *21*, 4084−4089. (g) Li, L.; Metz, M. V.; Li, H.; Chen, M.-C.; Marks, T. J.; Liable-Sands, L.; Rheingold, A. L. *J. Am. Chem. Soc.* **2002**, *124*, 12725−12741. (h) Kunz, K.; Erker, G.; Doering, S.; Bredeau, S.; Kehr, G.; Fröhlich, R. *Organometallics* **2002**, *21*, 1031−1041. (i) Cavallo, L. *Catal. Met. Complexes* **2002**, *25*, 23−56. (j) Hair, G. S.; Jones, R. A.; Cowley, A. H.; Lynch, V. *Inorg. Chem.* **2001**, *40*, 1014−1019. (k) Jin, J.; Wilson, D. R.; Chen, E. Y.-X. *Chem. Commun.* **2002**, *7*, 708−709. (l) Leusen, D.; Beetstra, D. J.; Hessen, B.; Teuben, J. H. *Organometallics* **2000**, *19*, 4084−4089. (m) Stevens, J. C. In *Catalyst Design for Tailor-Made Polyolefins*; Soga, K., Teramo, M., Eds.; Elsevier: Amsterdam, 1994; p 277. (n) Klosin, J.; Kruper, W. J.; Nickias, P. N.; Roof, G. R.; Soto, J.; Graf, D. D. U.S. Patent Application U.S. No. 715,380, 2003. (o) Chum, P. S.; Kruper, W.; Guest, M. J. *Adv. Mater.* **2000**, *12*, 1759−1767. (p) Stevens, J. C. In *Studies in Surface Science and Catalysis*; Hightower, J. W., Delglass, W. N., Iglesia, E., Bell, A. T., Eds.; Elsevier: Amsterdam, 1996; Vol. 101, p 11.

(3) (a) Lee, S.-G.; Hong, S.-D.; Park, Y.-W.; Jeong, B.-G.; Nam, D.-W.; Jung, H. Y.; Lee, H.; Song, K. Ho. *J. Organomet. Chem.* **2004**, *689*, 2586−2592. (b) Kim, I.; Ha, C.-S. *Polym. Bull.* **2004**, *52*, 133−139. (c) Nomura, K.; Fujita, K.; Fujiki, M. *J. Mol. Catal. A: Chem.* **2004**, *220*, 133−144. (d) Resconi, L.; Cavallo, L.; Fait, L.; Fait, A.; Piemontesi, F. *Chem. Rev.* **2000**, *100*, 1253−1345.

(4) (a) Lahitte, J.-F.; Kaminsky, W.; Stojkovic, O.; Peruch, F.; Lutz, P. *J. Macromol. Rapid Commun.* **2004**, *25*, 1010−1014. (b) Ewart, S. W.; Sarsfield, M. J.; Jeremic, D.; Tremblay, T. L.; Williams, E. F. F.; Baird, M. C. *Organometallics* **1998**, *17*, 1502−1510. (c) Csok, Z.; Liguori, D.; Sessa, I.; Zannoni, C.; Zambelli, A. *Macromol. Chem. Phys.* **2004**, *205*, 1231−1237. (d) Gentil, S.; Pirio, N.; Meunier, P.; Gallou, F.; Paquette, L. A. *Eur. Polym. J.* **2004**, *40*, 2241−2246. (e) Yakota, Y.; Inoue, T.; Nagamura, S.; Shozaki, H.; Tomotsu, N.; Kuramoto, M.; Ishihara, N. In *Metalorganic Catalysts for Synthesis and Polymerization: Recent Results by Ziegler-Natta and Metallocene Investigations*; Kaminsky, W., Ed.; Springer-Verlag: Berlin, 1999; p 435.

(5) (a) Tritto, I.; Boggioni, L.; Sacchi, M. C.; Locatelli, P.; Ferro, D. R. *Macromol. Symp.* **2004**, *213*, 109−121. (b) Kaminsky, W.; Tran, P.-D.; Werner, R. *Macromol. Symp.* **2004**, *213*, 101−108. (c) Kim, E.-G.; Klein, M. L. *Organometallics* **2004**, *23*, 3319−3326. (d) Lavoie, A. R.; Ho, M. H.; Waymouth, R. M. *Chem. Commun.* **2003**, *7*, 864−865. (e) Rodriguez-Delgado, A.; Mariott, W. R.; Chen, E. Y.-X. *Macromolecules* **2004**, *37*, 3092−3100.

(6) (a) Ramos, J.; Munoz-Escalona, A.; Martinez, S.; Martinez-Salazar, J.; Cruz, V. *J. Chem. Phys.* **2005**, *122*, 074901/1−074901/4. (b) Cundari, T. R.; Taylor, C. D. *Organometallics* **2003**, *22*, 4047−4059. (c) Szabo, M. J.; Berke, H.; Weiss, T.; Ziegler, T. *Organometallics* **2003**, *22*, 3671−3677. (d) Michalak, A.; Ziegler, T. *Catal. Met. Complexes* **2002**, *25* (Computational Modeling of Homogeneous Catalysis), 57−78. (e) Firman, T. K.; Ziegler, T. *J. Organomet. Chem.* **2001**, *635*, 153−164. (f) Khoroshun, D. V.; Musaev, D. G.; Vreven, T.; Morokuma, K. *Organometallics* **2001**, *20*, 2007−2026.

(7) (a) Zhu, C.; Ziegler, T. *Inorg. Chim. Acta* **2003**, *345*, 1−7. (b) Froese, R. D. J.; Musaev, D. G.; Morokuma, K. *Organometallics* **1999**, *18*, 373−379. (c) Musaev, D. G.; Froese, R. D. J.; Morokuma, K. *New J. Chem.* **1997**, *21*, 1269−1282. (d) Koga, N.; Yoshida, T.; Morokuma, K. *Ziegler catalysts: recent scientific innovations and technological improvements;* Fink, G., Muelhaupt, R., Brintzinger, H. H., Eds.; Springer: Berlin, Germany, 1995; pp 275−89. (e) Fan, L.; Harrison, D.; Woo, T. K.; Ziegler, T. *Organometallics* **1995**, *14*, 2018−2026.

(8) (a) Lanza, G.; Fragalà, L. I.; Marks, T. J. *J. Am. Chem. Soc.* **2000**, *122*, 12764−12777. (b)Lanza, G.; Fragalà, I. L.; Marks, T. J. *Organometallics* **2002**, *21*, 5594−5612. (c) Zurek, E.; Ziegler, T. *Prog. Polym. Sci.* **2004**, *29*, 107−148. (d) Xu, Z.; Vanka, K.; Firman, T.; Michalak, A.; Zurek, E.; Zhu, C.; Ziegler, T. *Organometallics* **2002**, *21*, 2444−2453. (e) Ystenes, M.; Eilertsen, J. L.; Liu, J.; Ott, M.; Rytter, E.; Stovneng, J. A. *J. Polym. Sci., Part A: Polym. Chem.* **2000**, *38*, 3450. (f) Xu, Z.; Vanca, K.; Ziegler, T. *Macromol. Symp.* **2004**, *206*, 457−469. (g) Wondimagegn, T.; Xu, Z.; Vanca, K.; Ziegler, T. *Organometallics* **2004**, *23*, 3847−3852.

(9) (a) Yang, S. H.; Huh, J.; Yang, J. S.; Jo, W. H. *Macromolecules* **2004**, *37*, 5741−5751. (b) Milano, G.; Fiorello, G.; Guerra, G.; Cavallo, L. *Macromol. Chem. Phys.* **2002**, *203*, 1564−1572. (c) Petitjean, L.; Pattou, D.; Ruiz-Lopez, M.-F. *THEOCHEM* **2001**, *541*, 227−235. (d) Moscardi, G.; Resconi, L.; Cavallo, L. *Organometallics* **2001**, *20*, 1918−1931. (e) Morokuma, K.; Yoshida, T.; Koga, N.; Musaev, D. G. *Polym. Mater. Sci. Eng.* **1996**, *74*, 425. (f) Yu, Z.; Chien, J. C. W. *J. Polym. Sci., Part A: Polym. Chem.* **1995**, *33*, 1085−1094. (g) Castonguay, L. A.; Rappé, A. K. *J. Am. Chem. Soc.* **1992**, *114*, 5832−5842. (h) Moscardi, G.; Piemontesi, F.; Resconi, L. *Organometallics* **1999**, *18*, 5264−5275. (i) Yang, S. H.; Huh, J.; Jo, W. H. *Organometallics* **2006**, *25*, 1144−1150. (j) Caporaso, L.; Gracia-Budria, J.; Cavallo, L. *J. Am. Chem. Soc.* **2006**, *128*, 16649−16654. (k) Guerra, G.; Corradini, P.; Cavallo, L. *Macromolecules* **2005**, *38*, 3973−3976.

(10) (a) Linas, G. H.; Day, R. O.; Rausch, M. D.; Chien, J. C. W.; *Organometallics* **1993**, *12*, 1283−1288). (b) Gómez, F. J.; Waymouth, R. M. *Macromolecules* **2002**, *35*, 3358−3368. (c) Miller, S.; Bercaw, J. E. *Organometallics* **2002**, *21*, 934−945. (d) Lee, M. H.; Han, Y.; Kim, D.-h.; Hwang, J.-W.; Do, Y. *Organometallics* **2003**, *22*, 2790−2796. (e) Miller, S.; Bercaw, J. E. *Organometallics* **2006**, *25*, 3576−3592.

(11) (a) Cavallo, L.; Guerra, G.; Vacatello, M.; Corradini, P. *Macromolecules* **1991**, *24*, 1784−1790. (b) Hölscher, M.; Keul, H.; Höocker, H. *Chem.−Eur. J.* **2001**, *7*, 5419−5426. (c) Yoshida, T.; Koga, N.; Morokuma, K. *Organometallics* **1996**, *15*, 766−777. (d) L.; Guerra, G.; Vacatello, M.; Corradini, P. *Macromolecules* **1996**, *29*, 4834−4845.

(12) (a) Wieser, U.; Schaper, F.; Brintzinger, H.-H. *Macromol. Symp.* **2006**, *236*, 63−68. (b) Busico, V.; Cipullo, R.; Cutillo, F.; Friederichs, N.; Ronca, S.; Wang, B. *J. Am. Chem. Soc.* **2003**, *125*, 12402−12403. (c) Chen, Y.-X.; Kruper, W. J.; Roof, G.; Wilson, D. R. *J. Am. Chem. Soc.* **2001**, *123*, 745−746. (d) Coevoet, D.; Cramail, H.; Deffieux, A. *Macromol. Chem. Phys.* **1998**, *199*, 1459−1464. (e) Harlan, C. J.; Bott, S. G.; Barron, A. R. *J. Am. Chem. Soc.* **1995**, *117*, 6465−6474. (f) Sishta, C.; Harthorn, R.; Marks, T. J. *J. Am. Chem. Soc.* **1992**, *114*, 1112−1114. (g) Pasynkiewicz, S. *Polyhedron* **1990**, *9*, 429. (h) Reddy, S. S.; Sivaram, S. *Prog. Polym. Sci.* **1995**, *20*, 309−367.

(13) (a) Schlögl, M.; Riethmueller, S.; Troll, C.; Möller, M.; Rieger, B. *Macromolecules* **2004**, *37*, 4004−4007. (b) Metz, M. V.; Schwartz, D. J.; Stern, C. L; Marks, T. J.; Nickias, P. N. *Organometallics* **2002**, *21*, 4159−4168. (c) Zhou, J.; Lancaster, S. J.; Walter, D. A.; Beck, S.; Thornton-Pett, M.; Bochmann, M. *J. Am. Chem. Soc.* **2001**, *123*, 223−237. (d) Chase, P. A.; Piers, W. E.; Patrick, B. O. *J. Am. Chem. Soc.* **2000**, *122*, 12911−12912. (e) Li, L.; Stern, C. L.; Marks, T. J. *Organometallics* **2000**, *19*, 3332−3337. (f) Luo, L.; Marks, T. J. *Top. Catal.* **1999**, *7*, 97−106. (g) Li, L.; Marks, T. J. *Organometallics* **1998**, *17*, 3996−4003. (h) Deck, P. A.; Beswick, C. L.; Marks, T. J. *J. Am. Chem. Soc.* **1998**, *120*, 1772−1784. (i) Piers, W. E.; Chivers, T. *Chem. Soc. Rev.* **1997**, *26*, 345−354. (j) Yang, X.; Stern, C. L.; Marks, T. J. *J. Am. Chem. Soc.* **1994**, *116*, 10015−10031. (k) Bochmann, M.; Lancaster, S. J.; Hursthous, M. B.; Malik, K. M. *Organometallics* **1994**, *13*, 2235−2243. (l) Yang, X. M.; Stern, C. L.; Marks, T. J. *J. Am. Chem. Soc.* **1991**, *113*, 3623−3625.

Scheme 1. Cossee−Arlman Mechanism for Olefin Polymerization

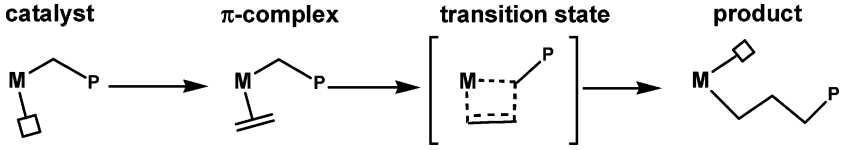

represents an important aspect of most early metal homogeneous polymerization processes. Indeed, there is growing experimental evidence that cocatalyst−counterion "fit" and solvation both play a significant role in the structures and energetics of the ion pairing, hence, in polymerization activities and selectivities. Ion pairs are typically formed using neutral group 13 organo-Lewis acids such as methylalumoxane (MAO),[12] BAr^F_3, and $AlAr_3^F$ reagents (Ar^F = fluoroaromatic group)[13] or saltlike activators such as $Ph_3C^+X^-$, $HNR_3^+X^-$, and Fc^+X^- (X^- = $BAr^F{}_4^-$, $AlAr^F{}_4^-$, $M(OAr^F)_n^-$) reagents.[14] MAO represents a weakly coordinating counteranion precursor which also acts as a scavenger for impurities and an alkylating and chain transfer agent and is thought to inhibit catalyst deactivation via bimolecular reductive hydrogen transfer.[1,12] Nevertheless, MAO is expensive, and its complex nature hampers unambiguous structural/dynamic characterization, thus precluding rational tuning of catalyst properties. In contrast, borane[13] and borate[14] cocatalysts yield structurally well-defined cation−anion pairs with moderate to very high polymerization activities,[1,13,14] in some cases exhibiting productivities greater than those of MAO-activated systems,[2e] and in addition tolerating some classes of functionalized olefins.[15] Importantly, structurally well-defined catalysts allow systematic studies of thermochemistry, metrical parameters, and solution structural dynamics, providing insight into the nature of cation−anion interactions as well as into the kinetics of polymerization.[16−21]

Within this scenario, the goal of the present study is to provide the first detailed analysis of stereochemical relationships governing polypropylene chain propagation processes in C_1-symmetric CGCTi-mediated propylene polymerization. Emphasis here focuses on processes at the naked CGCTi−R^+ cation, with counterion/cocatalyst/activator influence also examined for the analogous ethylene insertion process. Nonstereogenic counterion interactions were previously analyzed for ethylene insertion in the simpler, more symmetrical C_s-symmetric (H_2-SiCpN^{t}Bu)(R)Ti−$CH_3^{+\cdots}H_3CB(C_6F_5)_3^-$ system[8a,b] and serve as a reference point. In the present study, it is especially informative to extend the analysis of counterion interactions to both active sites of the CGC C_1-symmetric catalyst. In C_s-symmetric catalysts, the two catalytic sites are symmetry-equivalent, while, in C_1-symmetric catalysts, the two active sites are diastereotopic and, therefore, have intrinsically different reactivities. Solvation effects are also investigated here by comparing gas-phase energetics with those in solution. In marked contrast to many other single-site catalysts,[1,13,14] it will be seen here that the counteranion/cocatalyst strongly modulates enchainment rates but not stereochemistry and that the latter is dominated by the interplay between monomer−ancillary ligand and monomer−polymeryl fragment nonbonded interactions.

Computational Details

DFT calculations were performed using the B3LYP formalism. The effective core potential (ECP) of Hay and Wadt,[22] which explicitly treats 3s and 3p electrons and a basis set contracted as [3s,3p,3d] were used for the Ti atom. The standard all-electron 6-31G basis was used for the remaining atoms.[23] Molecular geometry optimization of stationary

(14) (a) Metz, M. V.; Sun, Y.; Stern, C. L; Marks, T. J. *Organometallics* **2002**, *21*, 3691−3702. (b) Chen, Y.-X.; Marks, T. J. *J. Am. Chem. Soc.* **2001**, *123*, 11803−11804. (c) Sun, Y.; Metz, M. V.; Stern, C. L.; Marks, T. J. *Organometallics* **2000**, *19*, 1625−1627. (d) Metz, M. V.; Schwartz, D. J.; Stern, C. L.; Nickias, P. N.; Marks, T. J. *Angew. Chem., Int. Ed.* **2000**, *39*, 1312−1316. (e) Chen, Y.-X.; Stern, C. L.; Marks, T. J. *J. Am. Chem. Soc.* **1997**, *119*, 2582−2583. (f) Jia, L.; Yang, X.; Stern, C. L.; Marks, T. J. *Organometallics* **1997**, *16*, 842−857. (g) Chien, J. C. W.; Tsai, W.-M.; Rausch, M. D. *J. Am. Chem. Soc.* **1991**, *113*, 8570−8571. (h) Yang, X.; Stern, C. L.; Marks, T. J. *Organometallics* **1991**, *10*, 840−842. (i) Ewen, J. A.; Elder, M. J.; Ewen, J. A.; Elden, M. J. European Patent Appl. p 426637 1991. (j) Hlatky, G. G.; Upton, D. J.; Turner, H. W. U.S. Patent Appl. p 459921 1990.

(15) (a) Xu, G.; Chung, T. C. *Macromolecules* **2000**, *33*, 5803−5809. (b) Xu, G.; Chung, T. C. *Macromolecules* **1999**, *32*, 8689−8692. (c) Xu, G.; Chung, T. C. *J. Am. Chem. Soc.* **1999**, *121*, 6763−6764. (d) Chung, T. C.; Janvikul, W. *J. Organomet. Chem.* **1999**, *581*, 176−187. (e) Koo, K.; Marks, T. J. *J. Am. Chem. Soc.* **1998**, *120*, 4019−4020. (f) Collins, S.; Ward, D. G.; Suddaby, K. H. *Macromolecules* **1994**, *27*, 7222−7224. (g) Deng, H.; Shiono, T.; Soga, K. *Macromolecules* **1995**, *27*, 3067−3073. (h) Collins, S.; Ward, D. G. *J. Am. Chem. Soc.* **1992**, *114*, 5460−5462.

(16) (a) Hannig, F.; Fröhlich, R.; Bergander, K.; Erker, G.; Petersen, J. L. *Organometallics* **2004**, *23*, 4495−4502. (b) Strauch, J. W.; Faure, J.-L.; Bredeau, S.; Wang, C.; Kehr, G.; Froehlich, R.; Luftmann, H.; Erker, G. *J. Am. Chem. Soc.* **2004**, *126*, 2089−2104. (c) Erker, G. *Acc. Chem. Res.* **2001**, *34*, 309−317. (d) Dahlmann, M.; Erker, G.; Bergander, K. *J. Am. Chem. Soc.* **2000**, *122*, 7986−7998. (e) Dahlmann, M.; Erker, G.; Nissien, M.; Fröhlich, R. *J. Am. Chem. Soc.* **1999**, *121*, 2820−2828. (f) Karl, J.; Dahlmann, M.; Erker, G.; Bergander, K. *J. Am. Chem. Soc.* **1998**, *120*, 5643−5652. (g) Temme, B.; Erker, G.; Karl, J.; Luftmann, H.; Fröhlich, R.; Kotila, S. *Angew. Chem., Int. Ed. Engl.* **1995**, *34*, 1755−1757.

(17) (a) Carpentier, J.-F.; Maryin, V. P.; Luci, J.; Jordan, R. F. *J. Am. Chem. Soc.* **2001**, *123*, 898−909. (b) Carpentier, J.-F.; Wu, Z.; Lee, W. C.; Strömberg, S.; Christopher, J. N.; Jordan, R. F. *J. Am. Chem. Soc.* **2000**, *122*, 7750−7767. (c) Casey, C. P.; Carpenetti, D. W., II. *Organometallics* **2000**, *20*, 3970−3977. (d) Casey, C. P.; Carpenetti, D. W., II; Sakurai, H. *J. Am. Chem. Soc.* **1999**, *121*, 9483−9484. (e) Abrams, M. B.; Yoder, J. C.; Loeber, C.; Day, M. V.; Bercaw, J. E. *Organometallics* **1999**, *18*, 1389−1401. (f) Galakhov, M. V.; Heinz, G.; Royo, P. *Chem. Commun.* **1998**, 17−18. (g) Casey, C. P.; Fagan, M. A.; Hallenbeck, S. L. *Organometallics* **1998**, *17*, 287−289. (h) Casey, C. P.; Hallenbeck, S. L.; Wright, J. M.; Landis, C. R. *J. Am. Chem. Soc.* **1997**, *119*, 9680−9690. (i) Temme, B.; Karl, J.; Erker, G. *Chem.−Eur. J.* **1996**, *2*, 919−924. (j) Casey, C. P.; Hallenbeck, S. L.; Pollock, D. W.; Landis, C. R. *J. Am. Chem. Soc.* **1995**, *117*, 9770−9771. (k) Wu, Z.; Jordan, R. F. *J. Am. Chem. Soc.* **1995**, *117*, 5867−5868.

(18) (a) Bryliakov, K. P.; Babushkin, D. E.; Talsi, E. P.; Voskoboynikov, A. Z.; Gritzo, H.; Schroeder, L.; Damrau, H.-R. H.; Wieser, U.; Schaper, F.; Brintzinger, H. H. *Organometallics* **2005**, *24*, 894−904. (b) Beck, S.; Lieber, S.; Schaper, F.; Geyer, A.; Brintzinger, H.-H. *J. Am. Chem. Soc.* **2001**, *123*, 1483−1489. (c) Beck, S.; Prosenc, M.-H.; Brintzinger, H.-H. *J. Mol. Catal. A: Chem.* **1998**, *128*, 41−52.

(19) (a) Beswick, C. L.; Marks, T. J. *J. Am. Chem. Soc.* **2000**, *122*, 10358−10370. (b) Chen, Y.-X.; Marks, T. J. *Chem. Rev.* **2000**, *100*, 1391−1434. (c) Beswick, C. L.; Marks, T. J. *Organometallics* **1999**, *18*, 2410−2412. (d) Chen, Y.-X.; Metz, M. V.; Li, L.; Stern, C. L.; Marks, T. J. *J. Am. Chem. Soc.* **1998**, *120*, 6287−6305. (e) Chen, Y.-X.; Stern, C. L.; Yang, S. T.; Marks, T. J. *J. Am. Chem. Soc.* **1996**, *118*, 12451−12452. (f) Giardello, M. A.; Eisen, M. S.; Stern, C. L.; Marks, T. J. *J. Am. Chem. Soc.* **1995**, *117*, 12114−12129. (g) Deck, P. A.; Marks, T. J. *J. Am. Chem. Soc.* **1995**, *117*, 6128−6129.

(20) (a) Liu, Z.; Somsook, E.; White, C. B.; Rosaaen, K. A.; Landis, C. R. *J. Am. Chem. Soc.* **2001**, *123*, 11193−11207. (b)Beck, S.; Brintzinger, H.-H.; Suhm, J.; Mülhaupt, R. *Macromol. Rapid Commun.* **1998**, *19*, 235−239. (c) Eisch, J.J.; Pombrik, S.I.; Gurtzgen, S.; Rieger, R., Huzier, W. In *Catalyst Design for Tailor-Made Polyolefins*; Soga, K., Teramo, M., Eds.; Elsevier: Amsterdam, 1994; p 221.

(21) (a) Feichtinger, D.; Plattner, D. A.; Chen, P. *J. Am. Chem. Soc.* **1998**, *120*, 7125−7126. (b) Richardson, D. E.; Alameddin, N. G.; Ryan, M. F.; Hayes, T.; Eyler, J. R.; Siedle, A. R. *J. Am. Chem. Soc.* **1996**, *118*, 11244−11253. (c) Alameddin, N. G.; Ryan, M. F.; Eyler, J. R.; Siedle, A. R.; Richardson, D. E. *Organometallics* **1995**, *14*, 5005−5007.

(22) Hay, P. J.; Wadt, W. R. *J. Chem. Phys.* **1985**, *82*, 299−310.

(23) (a) Hehre, W. J.; Ditchfield, R.; Pople, J. A. *J. Chem. Phys.* **1972**, *56*, 2257−2261. (b) Francl, M. M.; Pietro, W. J.; Hehre, W. J.; Binkley, J. S.; Gordon, M. S.; DeFrees, D. J.; Pople, J. A. *J. Chem. Phys.* **1982**, *77*, 3654−3665.

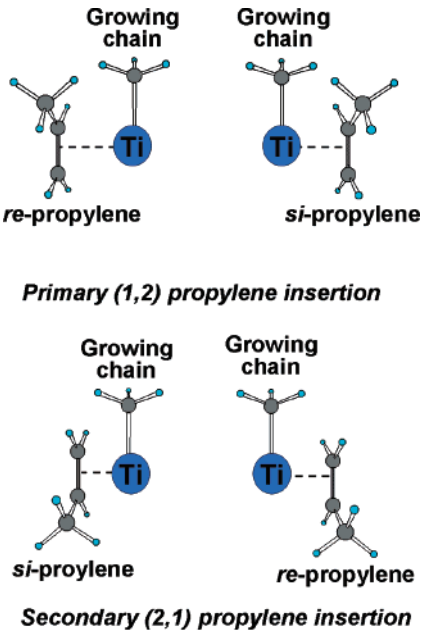

Figure 1. Four possible insertion modes of a prochiral olefin into a Ti−CH_3 growing chain.

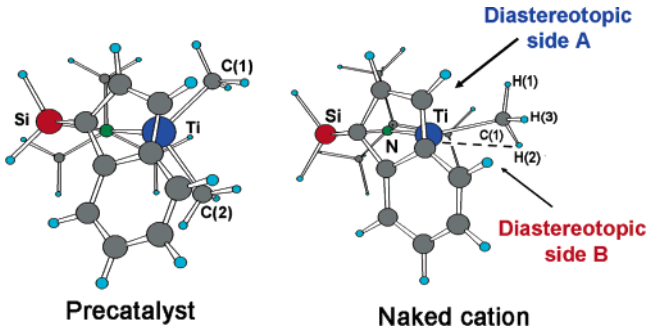

Figure 2. Structure of the $H_2Si(ind)(^tBuN)Ti(CH_3)_2$ precatalyst and of the activated catalyst $H_2Si(ind)(^tBuN)TiCH_3^+$ naked cation.

points used analytical gradient techniques. No local symmetry and no geometrical constrains were imposed in optimization.

The "distinguished reaction coordinate procedure" was used in determining the transition state geometry for the ethylene and propylene insertion processes, and the reaction coordinate was associated with the vector along the evolving new C—C σ bond (Ti—$CH_3 \cdots$ RHC═CHR′). Energetic profiles were constructed along this vector, optimizing all the other geometrical parameters without any constraints. For ethylene insertion, computed SCF energies (ΔE) were corrected for thermal and zero-point vibrational energies ($\Delta H°_{298}$) and entropies ($\Delta S°_{298}$) to obtain the free energy change ($\Delta G°_{298}$) at 298 K. Frequency analyses were performed to obtain thermochemical information. Force constants were determined analytically. Solvent effects were modeled using the Polarized Continuum (overlapping spheres) formalism (PCM) of Tomasi and co-workers.[24] The PCM method models solvation as a continuum of a uniform dielectric constant, and the solute is immersed in a cavity within the solvent. The cavity is constructed by placing a sphere around each solute heavy atom. Hydrogen atoms are always enclosed in the sphere of the atom to which they are bonded. For the atomic radii, the UAHF approximation was used. In this method, the

(24) (a) Miertus, S.; Tomasi, J. *Chem. Phys.* **1982**, *65*, 239−245. (b) Miertus, S.; Scrocco, E.; Tomasi, J. *Chem. Phys.* **1981**, *55*, 117−129. (c) Cossi, M.; Barone, V.; Cammi, R.; Tomasi, J. *Chem. Phys. Lett.* **1996**, *255*, 327−335. (d) Cances, M. T.; Mennucci, V.; Tomasi, J. *J. Chem. Phys.* **1997**, *107*, 3032−3041. (e) Barone, V.; Cossi, M.; Tomasi, J. *J. Comput. Chem.* **1998**, *19*, 404−417.

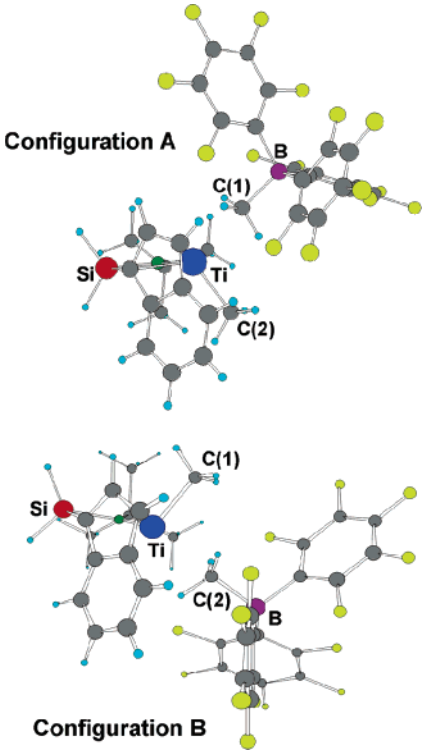

Figure 3. Structures of the activated $H_2Si(ind)(^tBuN)TiCH_3^+$ $H_3CB(C_6F_5)_3^-$ contact ion pair.

effects of solvation are folded into the iterative SCF procedure. The dielectric constant of toluene is 2.379. All calculations were performed using the G98[25] code on IBM-SP and Origin 3000 systems.

Results and Discussion

This section begins with a discussion of the computed molecular structure and bonding in the neutral C_1-symmetric dialkyl $H_2Si(ind)(^tBuN)Ti(CH_3)_2$ precatalyst. These results are then compared and contrasted with those for the "naked" monoalkyl cation prepared by alkyl anion abstraction. Next, the neutral dialkyls are "activated" with $B(C_6F_5)_3$ to yield the catalytically active cation−anion contact pair. The structure of the ion pair is analyzed and compared with that of the "naked" monoalkyl cation. Then, the energetics of the abstraction process are analyzed and compared to experiment. The energetics of the heterolytic ion pair separation process are next scrutinized, and the effects of the solvent environment are assessed. Then, olefin insertion processes are scrutinized assuming that a variant of the classic Cossee−Arlman mechanism[26] is operative (e.g., Scheme 1), involving (i) olefin coordination to a vacant catalytic site and (ii) alkyl migration of the σ-coordinated growing chain to the π-coordinated olefin.

Thermodynamic aspects of the reaction profile for ethylene insertion at $H_2Si(ind)(^tBuN)TiCH_3^+$ are first investigated. We compare the energetic profiles for ethylene insertion at the naked cation with that at the ion pair adduct to understand counterion effects. It will be seen that the presence of the counterion, although affecting the enchainment barrier, does not appreciably influence enchainment stereochemistry and, hence, polymer microtacticity in this particular case. Next, ethylene insertion

(25) Frisch, M. J., et al. *GAUSSIAN-98*; Gaussian Inc.: Pittsburgh, PA, 1995.
(26) (a) Cossee, P. *J. Catal.* **1964**, *3*, 80−88. (b) Arlman, E. J.; Cossee, P. *J. Catal.* **1964**, *3*, 99−104.

Table 1. Selected Bond Lengths (Å), Bond and Torsion Angles (deg) in the $H_2Si(ind)(^tBuN)Ti(CH_3)_2$ Precatalyst, in the $H_2Si(ind)(^tBuN)TiCH_3^+$ Naked Cation, and in the $H_2Si(ind)(^tBuN)TiCH_3^+$ $H_3CB(C_6F_5)_3^-$ Contact Ion Pair

			contact ion pair	
	precatalyst	naked cation	conf. A	conf. B
	Bond Length (Å)			
Ti−Cp_{centr}	2.217 (2.045)[a]	2.092	2.159	2.201
Ti−C(1)	2.081	2.048	2.366	2.071
Ti−C(2)	2.086		2.068	2.336
Ti−N	1.915 (1.915)[a]	1.847	1.888	1.878
N−Si	1.830 (1.739)[a]	1.887	1.845	1.849
C(1)−H(1)	1.101	1.103	1.092	1.095
C(1)−H(2)	1.098	1.107	1.098	1.099
C(1)−H(3)	1.096	1.093	1.098	1.099
C(1)−B			1.698	
C(2)−B				1.710
B−$C(C_6F_5)_{av}$			1.652	1.652
	Bond Angles (deg)			
Ti−N−Si	101.4 (106.9)[a]	98.8	102.0	100.1
C(1)−Ti−C(2)	100.7		100.4	95.7
Ti−C(2)−B			165.6	173.6
Ti−C(1)−H(1)	107.3	108.8	113.6	113.4
Ti−C(1)−H(2)	109.5	103.8	107.0	106.3
Ti−C(1)−H(3)	113.1	118.9	108.0	109.7
C(1)−B− $C(C_6F_5)_{av}$			108.5	
C(2)−B− $C(C_6F_5)_{av}$				107.6
	Torsion Angle (deg)			
C(1)−Ti−N−Si	55.9	14.2	46.1	65.9
C(2)−Ti−N−Si	53.4		60.9	36.5

[a] Data in parentheses refer to values from XRD analysis of $[(CH_3)_2Si(ind)(CHMePh)N]TiCl_2$ (ref 30).

at $H_2Si(ind)(^tBuN)Ti(^nC_3H_7)^+$ $H_3CB(C_6F_5)_3^-$ (second ethylene insertion) is analyzed to evaluate counteranion influence on the chain propagation barrier. These analyses are necessary for subsequent analysis of propylene insertion within the C_1-symmetric naked cation model. Prochiral propylene and higher α-olefins introduce stereoselection and regioselection intricacies. In fact, coordination of prochiral olefins such as propylene gives rise to non-superimposable conformers,[27] denoted *re* (rectus) and *si* (sinistrus) to distinguish olefin coordination motifs and to define the heterotopic half-spaces.[27] The two insertion modes are enantiotopic (enentiofacial selectivity or enantioselectivity), and every propylene insertion creates a new stereogenic center—the tertiary carbon atom configuration of the propagating chain adjacent to the metal center (see Figure S1 in the Supporting Information).[28] Multiple insertions of the same propylene enantioface produce isotactic polymer chains (Scheme S1a), while multiple insertions of alternating propylene enantiofaces produce syndiotactic polymer chains (Scheme S1b). Random enantioface insertions afford an atactic polymer chain (Scheme S1c). In this context, a propylene molecule can, in principle, coordinate and undergo insertion into a transition metal−carbon bond via four different pathways (Figure 1).

Whether olefin insertion is primary or secondary defines the enchainment regiochemistry, while the enantioface choice (or enantiofacial selectivity) defines the stereochemistry of each insertion. In the particular case considered in this work, a C_1-symmetric catalyst, a further chirality element is associated with the catalytic sites (Figure 2)—intrinsic chirality at the metal center, which can be denoted diastereotopic site A and B (Figure 2) to distinguish the diastereoisomeric olefin-bound intermediates which may arise upon interchanging relative positions of the growing chain and incoming monomer.[19f,29] In this context, we analyze regio- and stereochemical aspects of propylene insertion at the $H_2Si(ind)(^tBuN)TiR^+$ cation. Specifically, the intrinsic ability of the catalyst to direct optimum insertion routes is modeled by eq 1:

$$H_2Si(ind)(^tBuN)TiCH_3^+ + CH_2{=}CHCH_3 \quad \text{first insertion} \quad (1)$$

The effects on stereo- and regioselection in the polymeric chain propagation are then analyzed via eq 2:

$$H_2Si(ind)(^tBuN)Ti(^iBu)^+ + CH_2{=}CHCH_3 \quad \text{second insertion} \quad (2)$$

Here, the naked metal−isobutyl cation approximates the effects of a growing oligomer on enchainment.

Structure of the $H_2Si(ind)(^tBuN)Ti(CH_3)_2$ Precatalyst. Figure 2 shows a representation of the computed precatalyst structure, while Table 1 compiles significant metrical parameters and compares them to available experimental data.[30] The Ti metal center in the precatalyst has a pseudotetrahedral arrangement. Both Ti-bonded methyl groups are symmetrically disposed relative to the Ti−Cp_{centr}−Si plane and form an angle of 100.7° with the Ti center. In the precatalyst molecule, neither methyl group participates in an agostic interaction with the electron-deficient metal center which, in turn, exhibits approximate η^5-coordination to the indenyl ligand.

Structure of the $H_2Si(ind)(^tBuN)TiCH_3^+$ Naked Cation. The naked cation adopts a pseudo-trigonal-planar arrangement about the metal center (Figure 2; Table 1). The Ti−CH_3 bond is oriented slightly out of the Ti−N−Si plane (14.2°) and, relative to the parent precatalyst, is 0.03 Å shorter. The Ti−Cp_{centr} contact is similarly shorter (Δ = 0.13 Å). The DFT-derived bond angles and lengths involving the −Ti−CH_3 group are indicative of slight α-agostic interactions, thus deviating from local C_{3v} symmetry. All observed geometrical variations versus the molecular precursor clearly reflect the more electron-deficient character of the naked cation. As in the precatalyst, there is approximate η^5-coordination of the indenyl ligand to the Ti.

Structure of the $H_2Si(ind)(^tBuN)TiCH_3^+$ $H_3CB(C_6F_5)_3^-$ Catalyst−Cocatalyst Contact Ion Pair. Two configurations are possible here, depending on the coordination site of the counteranion at the Ti center (Figure 3 A,B). The Ti center activated by the $B(C_6F_5)_3$ cocatalyst possesses, in both cases, a pseudotetrahedral coordination geometry with asymmetrically bonded alkyl ligands (Table 1). The CH_3−Ti−CH_3 angle, however, remains nearly constant (∼100° in both configurations)

(27) Hanson K. R. *J. Am. Chem. Soc.* **1966**, *88*, 2731−2742.
(28) (a) Chan R. S.; Ingold C.; Prelog V. *Angew. Chem., Int. Ed. Engl.* **1966**, *5*, 385−415. (b) Prelog, V.; Helmchen, G. *Angew. Chem.* **1982**, *94*, 614−631.
(29) (a) Esteb, J. J.; Bergeron, M.; Dormady, C. N.; Chien, J. C. W.; Rausch, M. D. *J. Organomet. Chem*. **2003**, *675*, 97−104. (b) Aeby, A.; Consiglio, G. *Inorg. Chim. Acta* **1999**, *296*, 45−51. (c) Averbuj, C.; Tish, E.; Eisen, M. S. *J. Am. Chem. Soc.* **1998**, *120*, 8640−8646. (d) Arndt, M.; Beulich, I. *Macromol. Chem. Phys.* **1998**, *199*, 1221−1232. (e) Obora, Y.; Stern, C. L.; Marks, T. J.; Nickias, P. N. *Organometallics* **1997**, *16*, 2503−2505. (f) Kaminsky, W.; Arndt, M.; Beulich, I. *Polym. Mater. Sci. Eng.* **1997**, *76*, 18−19. (g) Chen, Y.-X.; Rausch, M. D.; Chien, J. C. W. *J. Organomet. Chem.* **1995**, *497*, 1−9. (h) Giardello, M. A.; Conticello, V. P.; Brard, L.; Gagne, M. R.; Marks, T. J. *J. Am. Chem. Soc.* **1994**, *116*, 10241−10254.
(30) McKnight, A. L.; Masood, M. A.; Waymouth R. M.; Strauss, D. A. *Organometallics*, **1997**, *16*, 2879−2885.

Table 2. Calculated Ion Pair Formation Enthalpies (kcal/mol) for the Process $H_2Si(R)(R^INH)TiCH_3 + B(C_6F_5)_3 \rightarrow H_2Si(R)(R^INH)TiCH_3^+H_3CB(C_6F_5)_3^- + \Delta H_{form}$ and Heterolytic Ion Pair Separation Enthalpies (kcal/mol) for the Process $H_2Si(R)(R^INH)TiCH_3^+H_3CB(C_6F_5)_3^- \rightarrow H_2Si(R)(R^INH)TiCH_3^+ + H_3CB(C_6F_5)_3^- + \Delta H_{ips}$

		ion pair formation ΔH_{form}			ion pair separation ΔH_{ips}		
		gas	toluene[a]	benzene[b]	gas	toluene[a]	benzene[b]
$H_2Si(ind)(^tBuN)TiCH_3^+$ $H_3CB(C_6F_5)_3^-$	**DFT**	−9.4[a]	−8.6		82.7[a]	45.5	
$H_2Si(C_5H_4)(CH_3N)TiCH_3^+$ $H_3CB(C_6F_5)_3^-$	**HF** MP2/BSSE	−10.0[b]		−13.0	83.0[b]		47.0
$H_2Si(C_5H_4)(^tBuN)TiCH_3^+$ $H_3CB(C_6F_5)_3^-$	**HF** MP2/BSSE	−10.0[b]		−13.0	78.0[b]		43.0

[a] Pathways A and B give indistinguishable results. [b]Values from ref 8a.

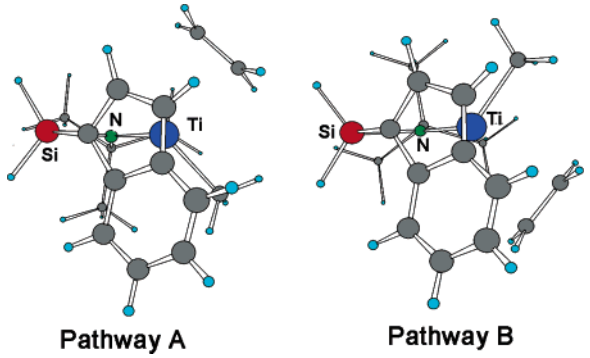

Figure 4. Ethylene insertion modes at the $H_2Si(ind)(^tBuN)TiCH_3^+$ cation.

upon $B(C_6F_5)_3$ coordination, while the activated Ti−CH_3 bond length undergoes considerable elongation (ΔTi−C ≈ 0.3 Å in both configurations) versus the precatalyst. Furthermore, the methyl H atoms undergo conformational inversion, forming a μ^3 bridge with the cationic Ti center, and having an approximately linear Ti · · · H_3C−B vector ($\angle$Ti−C−B = 165.6° and 173.6° in configuration **A** and **B**, respectively). The B atom assumes a pseudotetrahedral coordination environment, reflecting reorganization of the $B(C_6F_5)_3$ trigonal plane.

Energetics of Ion Pair Adduct Formation and Heterolytic Ion Pair Separation. The formation of the catalyst−cocatalyst contact ion pair with $B(C_6F_5)_3$ (eq 3) is computed to be exothermic (Table 2).

$$H_2Si(ind)(^tBuN)Ti(CH_3)_2 + B(C_6F_5)_3 \rightarrow H_2Si(ind)(^tBuN)TiCH_3^+ H_3CB(C_6F_5)_3^- + \Delta H_{form} \quad (3)$$

In accord with earlier results on the parent Me_4C_5 system,[8a,b] it can be seen (Table 2) that the solvent dielectric constant only slightly modifies (Δ = 0.8 kcal/mol) the electrostatics of ion pair formation. The gas-phase ion pair separation reaction (eq 4) is computed to be strongly endothermic and solvation-sensitive.

$$H_2Si(ind)(^tBuN)TiCH_3^+H_3CB(C_6F_5)_3^- \rightarrow H_2Si(ind)(^tBuN)TiCH_3^+ + H_3CB(C_6F_5)_3^- + \Delta H_{ips} \quad (4)$$

Calculated ion pair separation energies (E_{ips}) in the gas phase and in toluene are compiled in Table 2 and compared with literature data.[8a,b] Ion pair interactions may in principle play a significant role in catalyst stereoselectivity. In general, single-site catalysts (metallocene, ansa-bridged, CGC) used in homogeneous polymerizations have two possible sites for olefin activation/enchainment. If both sites are equally accessible, it is possible to obtain syndiotactic polymers with a C_s-symmetric catalyst. In these cases, olefin insertion is accompanied by

Table 3. Calculated SCF Energetic and Thermodynamic Pathways (kcal/mol) for Ethylene Insertion at the $H_2Si(ind)(^tBuN)TiCH_3^+$ Naked Cation[a,b]

	pathway A	pathway B		
	ΔE	ΔE	ΔH	ΔG
π-complex	−18.5	−18.8	−17.1	−5.9
TS	−9.6 (8.9)	−11.3 (7.5)	−9.7 (7.4)	4.4 (10.3)
products	−25.1	−26.2	−22.9	−9.3

[a] Values are referenced to reactants. [b]Values in parentheses refer to activation barriers.

"swinging" of the polymeryl chain and, hence, displacement of the counteranion from one site to the other on each olefin activation/enchainment. In principle, the strength of the ion pair interaction can modulate chain swinging, leaving only a single active site and transforming polymerization syndioselectivity into isoselectivity. The Zr-based C_s-symmetric CGC system $Me_2Si(Flu)(^tBuN)ZrCl_2$, for example, is reported to produce syndiotactic polypropylene with an MAO cocatalyst and isotactic polypropylene with a $B(C_6F_5)_4^-$ counteranion.[31] In other cases, the counteranion appears not to influence catalyst stereoselectivity. Thus, the Ti-based CGC system, $Me_2Si(Flu)(^tBuN)TiR_2$, invariably produces a syndiotactic polymer, with either MAO or $B(C_6F_5)_3$ as the cocatalyst.[32] This difference in behavior is undoubtedly associated with varying ion pairing strengths. In the Ti-based CGC catalyst, this interaction is sufficiently weak to allow insertion in concert with facile counteranion/chain swinging. In C_s-symmetric $Me_2C(Cp)(Flu)Zr-R^+$ catalysts, counteranion effects on propylene syndioselection can be very large.[33]

In our earlier analysis of $CGCTiCH_3^+$ ion pair interactions,[8a] it was shown that the $Ti^+ \cdots H_3CB(C_6F_5)_3^-$ contact is overwhelmingly electrostatic in character and that even considerable Ti · · · B elongations leave residual stabilization energies. In addition, solvation drastically reduces the ion pairing strength (Table 2), allowing greater counteranion mobility. The important catalytic consequence is that the $Ti^+ \cdots H_3CB(C_6F_5)_3^-$ contact can flexibly rearrange to allow greater ion pair separations, affording marked stereochemical mobility. Experimental support is found both in plausibly connected syndiotactic polymerization phenomenology[32] and in dynamic NMR studies of ion-pair symmetrization processes in $[1,2\text{-}(CH_3)_2C_5H_3]_2ZrCH_3^+$ $H_3CB(C_6F_5)_3^-$

(31) Shiomura, T.; Asamuma, T.; Inoue, N. *Macromol. Rapid. Commun*. **1996**, *17*, 9−14.
(32) (a) Hagihara, H.; Shiono, T.; Ikeda, T. *Macromolecules* **1997**, *30*, 4783−4785. (b) Hagihara, H.; Shiono, T.; Ikeda, T. *Macromolecules* **1998**, *31*, 3184−3188.
(33) (a) Chen, M.-C.; Roberts, J. A. S.; Seyem, A. M.; Li, L.; Zuccaccia, C.; Stahl, N. G.; Marks, T. J. *Organometallics* **2006**, *25*, 2833−2850. (b) Chen, M. C.; Roberts, J. A.; Marks, T. J. *Organometallics* **2004**, *23*, 932−935. (c) Chen, M.-C.; Roberts, J. A.; Marks, T. J. *J. Am. Chem. Soc.* **2004**, *126*, 4605−4625. (d) Roberts, J. A. S.; Chen, M.-C.; Seyam, A. M.; Li, L.; Zuccaccia, C.; Stahl, N. G.; Marks, T. J. *J. Am. Chem. Soc.*, in press.

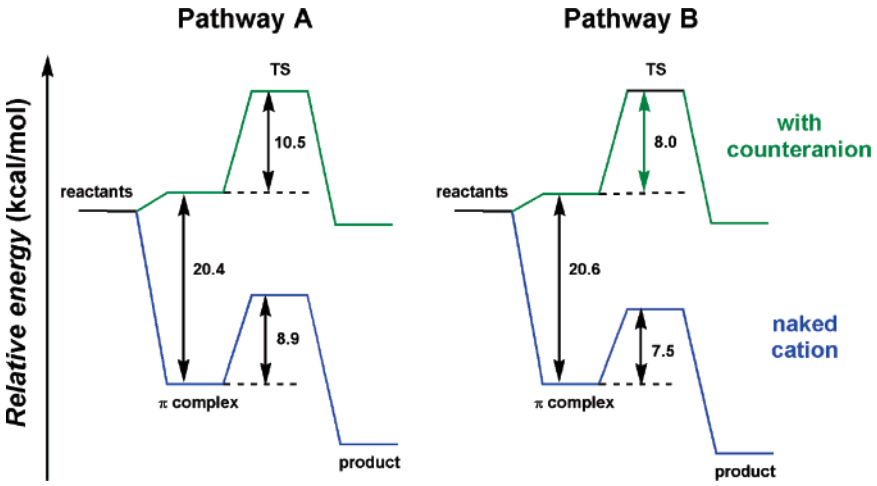

Figure 5. Comparison of ethylene insertion profiles at the naked cation and at the ion-pair adduct.

Scheme 2. Kinetics of the Chain Flipping Step versus the Ethylene Insertion Step

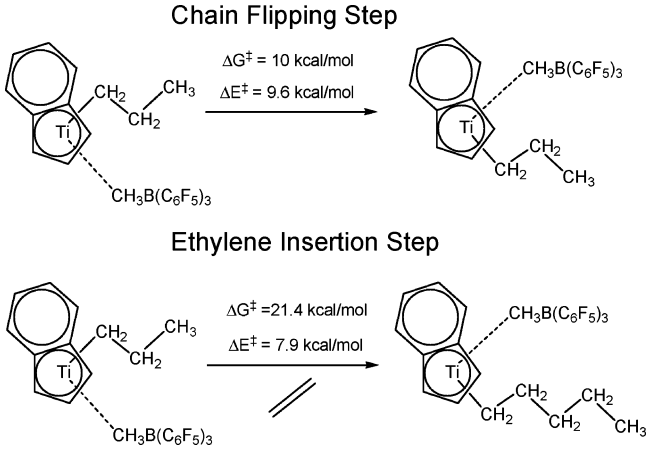

and similar complexes.[13g,14e,19a,c,34] These theoretical results agree well with experimental data on the counteranion role in Ti-based CGC stereoselectivity and confirm that the crucial role played by the catalyst asymmetry is well-represented by the naked cation. Further confirmation of the modest counteranion influence on stereoselectivity is presented below for ethylene insertion since this process represents the computationally and conceptually simplest model.

Ion Pair versus Naked Cation Description of Ethylene Insertion. The energetic aspects of ethylene insertion were first investigated at the $H_2Si(ind)(^tBuN)TiCH_3^+$ naked cation and then compared with those for ethylene insertion at the $H_2Si(ind)(^tBuN)TiCH_3^+H_3CB(C_6F_5)_3^-$ ion pair. As discussed above, there are two distinct pathways for olefin insertion into the Ti−CH_3 bond (**A** and **B)** due to the asymmetric ligation about the metal center (Figure 2). In pathway **A**, the growing chain (methyl group) lies proximal to the indenyl ring, while, in pathway **B**, the growing chain (methyl group) is distal to the indenyl group (Figure 4). In the cases of both ethylene and propylene insertions, only the frontside process is considered since it has been already demonstrated[8f] that frontside insertion is preferred over the backside process (Scheme S2). Pathway **A** incurs a slightly larger activation energy than pathway **B** ($\Delta E = 1.4$ kcal/mol) as a consequence of the greater steric crowding between the methyl group (growing chain) and the indenyl ring (Table 3).

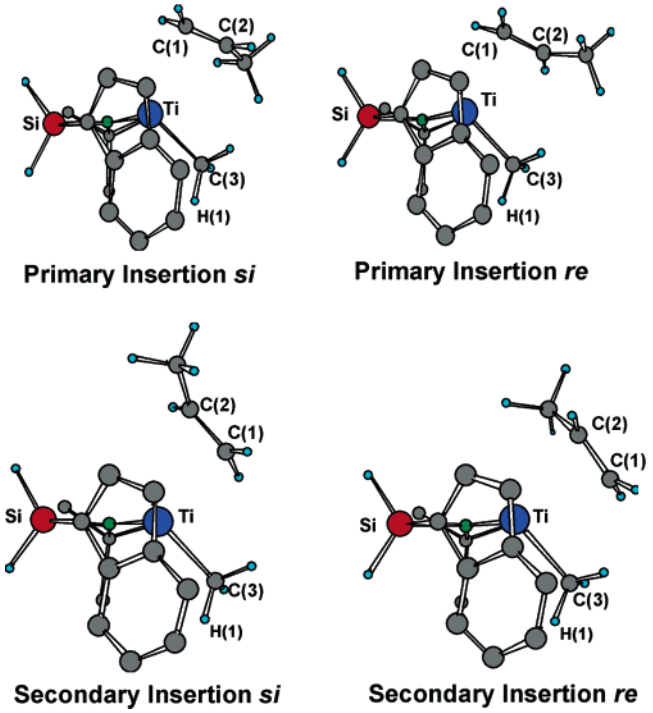

Figure 6. Possible propylene insertion pathways at $H_2Si(ind)(^tBuN)TiCH_3^+$ diastereotopic site **A** (see Figure S2 in the Supporting Information for the analogous insertions at diastereotopic site **B**).

This nonbonded repulsive effect is of even greater significance for longer polymer chains (*vide infra*). Importantly, the data in Table 3 argue that the kinetic aspects of the insertion process can be defined by SCF computation, since the Gibbs free energy values of the insertion barrier are very close to the SCF potential energies. Furthermore, the $-T\Delta S$ contribution remains almost constant along the π-complex → T.S. → product pathway.

Shifting the focus to the catalyst−cocatalyst ion pair, the computations indicate that the counteranion presence significantly affects polymerization activity. Effects have been analyzed for both pathways **A** and **B** to investigate whether the counteranion influence remains symmetric with respect to the diastereotopic active sites of the catalyst and, in turn, whether the C_1-symmetric catalyst−olefin chirality relationships (for propylene) are maintained in the presence of the $H_3CB(C_6F_5)_3^-$

counteranion. The results clearly indicate that the principal effect of the counteranion is a uniform displacement of the enchainment reaction coordinate to higher energies along both pathways, while the profiles associated with the metal−olefin π-complexes, transition states, and final kinetic products are similar to those for the naked catalyst cation (Figure 5). These results strengthen those from the earlier theoretical analysis of a *symmetrical* system,[8a,b] with the additional important implication here that ion pair formation has a major influence on catalytic activity but a far less dramatic influence on C_1-symmetric catalyst enchainment stereochemistry, hence product microstructure. This will be investigated further for propylene enchainment below.

To acquire better insight into counteranion/cocatalyst influence on ethylene enchainment at $H_2Si(ind)(^tBuN)Ti(^nC_3H_7)^+$ $H_3CB(C_6F_5)_3^-$, the second ethylene insertion process was also analyzed and counteranion effects on ethylene π-complex formation (ethylene uptake step) evaluated. Early studies have shown[8b,f] that, in the first ethylene insertion, the uptake step does not play any significant role in the overall kinetics. In contrast, Ziegler reported for a different Ti-based CGC catalyst that the counteranion presence influences the second ethylene uptake barrier in a kinetically significant manner.[8f] The present data (Table S1) confirm and extend these results since the uptake transition state is found to be energetically comparable to the insertion transition state. Moreover, solvation is found to have little effect on the energetic profile (Table S1). Note, however, that the stereoselection rules depend on the chirality relationships among the catalyst, the monomer, and the growing chain (*vide supra*) and, hence, these rules cannot be formally expressed in the uptake step.

The results presented so far argue that informative mechanistic analysis of prochiral olefin insertion stereochemistry at this particular C_1-symmetric catalytic center can benefit from the simpler, computationally more tractable naked cation approach. It should thereby be possible to isolate and explore, in detail and with greater computational efficiency, the relative cation-centered energetics of propylene enchainment pathways. Therefore, the following sections dealing with propylene insertion stereoselectivity will be discussed within the naked cation model. Note that any *complete* analysis of the counteranion influence on *all possible propylene insertion pathways* would require five geometry optimizations for each of the eight insertion modes. The total effort would hence require 34 optimizations for the first insertion and 36 optimizations for the second insertion (considering the redundant reactant geometries). This would be a task currently impracticable at any full QMC level.

Finally, the facile polymer chain swinging between the two catalytic sites (that has been found experimentally for the Ti-CGC based catalyst; *vide supra*) is highlighted by comparison of the kinetics of the insertion process and that of the polymer chain flipping step adopting a Ti−^{n}propyl group as the growing chain. It is seen that the enthalpic and, even more importantly, the entropic contribution (Table 3) as well as the counteranion effect (Figure 5) shift the SCF energy profile of the ethylene insertion to high energy, hence leading to a calculated energy barrier of 21.4 kcal/mol (Scheme 2). In the case of the polymer chain flipping step, the entropic contribution and the counteranion effect do not perturb the SCF energy profile in a significant manner, leading to an energy barrier of 10.0 kcal/mol (Scheme 2). These theoretical considerations together with the experimental evidence on the open nature of the CGC complexes (*vide supra*) strongly suggest that in the Ti-CGC based systems the chain swinging is kinetically favored and, hence, the two catalytic sites are kinetically accessible.

Table 4. Selected Computed Bond Lengths (Å), Bond and Torsion Angles (deg) of the π-Complex, Insertion Transition State, and Product for Insertions of Propylene at the $H_2Si(ind)(^tBuN)TiCH_3^+$ Cation (First Insertions)[a]

	pathway A				pathway B			
	primary		secondary		primary		secondary	
	si	*re*	*si*	*re*	*si*	*re*	*si*	*re*
				π-Complex				
Ti-Cp_{centr}	2.175	2.157	2.154	2.174	2.176	2.162	2.196	2.185
Ti−C(1)	2.423	2.521	2.445	2.423	2.459	2.440	2.416	2.444
Ti−C(2)	2.951	2.976	2.976	2.948	2.977	3.020	2.953	2.888
Ti−C(3)	2.058	2.060	2.058	2.063	2.064	2.062	2.062	2.063
C(3)−H(1)	1.093	1.094	1.093	1.094	1.097	1.096	1.095	1.096
Ti−C(3)−H(1)	114.9	113.7	115.7	113.5	112.2	112.5	114.2	112.9
C(3)−Ti,C(1)−C(2)	88.3	9.4	15.4	12.0	5.2	39.7	4.0	76.7
C(3)−(N−Ti−Cp_{centr})	56.4	55.0	55.8	57.1	56.9	56.9	58.8	56.2
				Transition State				
Ti−Cp_{centr}	2.164	2.173	2.170	2.180	2.160	2.156	2.174	2.269
Ti−C(1)	2.159	2.154	2.496	2.462	2.132	2.148	2.471	2.506
Ti−C(2)	2.533	2.537	2.233	2.222	2.525	2.531	2.213	2.225
Ti−C(3)	2.133	2.144	2.123	2.128	2.154	2.144	2.137	2.140
C(3)−H(1)	1.129	1.129	1.132	1.134	1.132	1.130	1.133	1.130
Ti−C(3)−H(1)	71.3	71.1	70.9	69.8	68.0	70.0	69.4	69.6
C(3)−Ti,C(1)−C(2)	14.7	0.0	13.0	19.3	7.5	13.2	15.7	6.9
C(3)−(N−Ti−Cp_{centr})	42.5	42.9	44.6	43.0	41.7	41.4	42.4	48.7
				Product				
Ti−Cp_{centr}	2.134	2.137	2.164	2.228	2.152	2.143	2.194	2.224
Ti−C(1)	2.034	2.042	2.485	2.461	2.037	2.027	2.458	2.451
Ti−C(2)	2.600	2.642	2.025	2.053	2.625	2.575	2.046	2.024
Ti−C(3)	2.452	2.412	2.459	2.424	2.397	2.468	2.428	2.483
C(3)−H(1)	1.114	1.110	1.117	1.118	1.110	1.119	1.120	1.121
Ti−C_α−C_β	91.5	93.1	86.3	84.2	92.5	90.7	84.3	84.8
Ti−C_α−C_β−C(3)	26.3	0.4	35.1	36.4	1.4	30.1	35.8	40.2

[a] Labeling refers to the structures in Figures 6, S2 and Scheme 3.

Propylene Insertion at $H_2Si(ind)(^tBuN)TiCH_3^+$ (First Insertion). For the first olefin insertion, there are four different pathways for each diastereotopic catalyst site (**A** and **B**), depending on the propylene methyl group orientation with respect to the Ti−CH_3 bond vector (Figure 6).

Activated Complex. Relevant computed metrical data for the intermediate $H_2Si(ind)(^tBuN)TiCH_3\cdots C_3H_6^+$ π-olefin complexes are summarized in Table 4. Along all reaction pathways, the Ti−CH_3 bond is oriented 55.0°−58.8° out of the Cp_{centr}−Ti−N plane (Table 4) and, therefore, the CH_3 group occupies one Ti coordination site while the π-bound olefin engages the second. The differing Ti−C contacts involving the metal center and the propylene π-bond indicate asymmetric bonding ($Ti-C(1)_{Av}$ = 2.446 Å, $Ti-C(2)_{Av}$ = 2.961 Å) due to both the propylene methyl group electronic effects and nonbonded repulsive interactions with the Cp ring.[8a,b] The remarkably different values of the C(3)−Ti,C(1)−C(2) torsion angles (Table 4) calculated for the various, nearly isoenergetic π complexes (Table S2) associated with the eight different enchainment pathways are indicative of a very flat potential energy surface for propylene rotation.

Nevertheless, the preferred geometry is found to involve a parallel/eclipsed arrangement of the olefin π bond and the Ti−C(1) σ bond.[34]

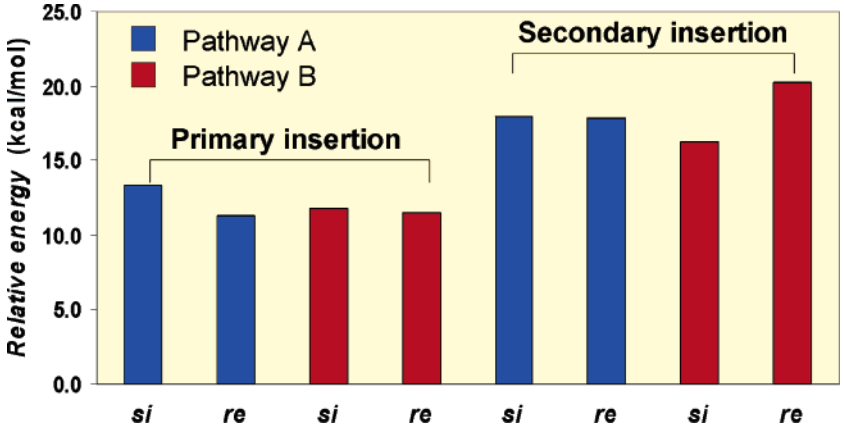

Figure 7. Energetic barriers for the first propylene insertion at $H_2Si(ind)(^tBuN)TiCH_3^+$ along the trajectories shown in Figures 6 and S2.

Scheme 3. Propylene First Insertion at the $H_2Si(ind)(^tBuN)TiCH_3^+$ Naked Cation for the Primary *re* Route

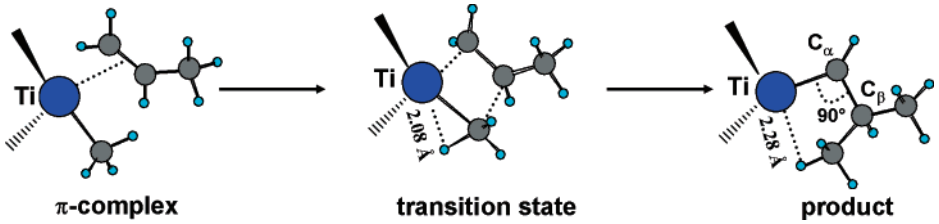

First Insertion Transition State. The transition state associated with the first propylene insertion at $H_2Si(ind)(^tBuN)TiCH_3^+$ involves a highly distorted $Ti-C(1)H_3$ conformation in all cases (Table 4), compared to both the naked methyl cation and the initial π-complex. Two of the $Ti-C(3)H_3$ hydrogen atoms become pseudo-eclipsed with respect to the approaching C═C fragment while the remaining H atom is involved in a strong α-agostic interaction (Scheme 3). Indeed, the interacting C(3)−H(1) bond length is significantly longer (1.13 Å) than the remaining C−H bonds (1.09 Å) in all pathways considered (Table 4). The geometries of the four-membered C(3)−Ti−C(1)−C(2) transition states exhibit a small folding angle (0.0°−19.3°), with puckering arising from methyl−propylene hydrogen atom repulsive interactions (Table 4).

First Insertion Product. The initial propylene enchainment product in all cases is found to have a γ-agostic structure with the $C(3)H_3$ chain-end group directed toward the vacant cationic Ti coordination site (Table 4). The small $Ti-C_\alpha-C_\beta-C(3)$ mean torsional angle (25.7°) indicates near coplanarity of the three σ bonds, hence, an eclipsed conformation of the $CH_2-CH_2-CH_3$ fragment. The $Ti-C_\alpha$ bond is bent out of the $Cp_{centr}-Ti-N$ plane, and the C(3)−H(1) σ bond is directed toward the vacant metal coordination site. Furthermore, $Ti-C_\alpha-C_\beta$ angle (∼90°) distortion relative to a tetrahedral arrangement (Scheme 3) and C(3)−H(1) bond elongation (Table 4) are observed as a consequence of the γ-agostic interaction. In the case of primary insertions along both **A** and **B** pathways, the $Ti-CH_2CH(CH_3)-CH_3^+$ isobutyl chain can, however, readily rearrange to an alternative β-agostic conformer by simple rotation (∼120°) about the C(1)−C(2) bond of the kinetic γ-product (*re* and *si* coordination). The CGC β-agostic conformers lie close in energy to the γ-agostic structures ($\Delta E \approx 1$ kcal/mol).

Energetics of the First Propylene Insertions. Energetic data for the first propylene insertion pathways are compiled in Table S2, and activation barriers are compared in Figure 7. The olefin coordination, i.e., formation of π-complexes, leads to comparable energetic stabilizations ($\Delta E = 20.5-21.9$ kcal/mol) for all pathways. The small differences among the pathways are correlated with the Ti−C(1) and Ti−C(2) distances (Table 4) and hence with the different degrees of metal center coordinative saturation. The activation energies (Figure 7) indicate that primary olefin insertion (1,2 regiochemistry) is favored. The barriers associated with primary insertions lie in the 11.3−13.3 kcal/mol range, while those for secondary insertions are ca. 5 kcal/mol greater (16.2−20.2 kcal/mol). These differences are primarily due to nonbonded interactions involving the propylene methyl group (Chart 1). In fact, for primary insertions, the propylene methyl group is oriented away from the catalyst center, thus favoring geometric relaxation. For 2,1 insertions, in contrast, the methyl group is placed in close proximity to the catalyst center, hence significantly enhancing nonbonded repulsions. The large differences between activation barriers for primary and secondary insertions suggest pronounced regioselectivity effects for the present CGC catalyst. In good agreement with these results, experimental polymer product NMR data[30] for the $(CH_3)_2Si(ind)(^tBuN)TiCl_2$/MAO + propylene system indicate only ∼2.8% 2,1 misinsertion errors.

The energetic stabilization associated with the enchainment products follows a trend analogous to that for the transition state energies (Table S2). In these products, steric effects are also responsible for the energetic differences between primary and

(34) (a) Stahl, N. G.; Salata, M. R.; Marks, T. J. *J. Am. Chem. Soc.* **2005**, *127*, 10898. (b) Zuccaccia, C.; Stahl, N. G.; Macchioni, A.; Chen, M.-C.; Roberts, J. A.; Marks, T. J. *J. Am. Chem. Soc.* **2004**, *126*, 1448. (c) Deck, P. A.; Beswick, C. L.; Marks. T. J. *J. Am. Chem. Soc.* **1998**, *120*, 1772. (d) Luo, L.; Marks, T. J. *Top. Catal.* **1999**, *7*, 97. (e) Chen, Y.-X.; Stern, C. L.; Marks, T. J. *J. Am. Chem. Soc.*, **1997**, *119*, 2582.
(35) Kawamura-Kuribayashi, H.; Koga, N.; Morokuma, K. *J. Am. Chem. Soc.* **1992**, *114*, 2359−2366.

Chart 1. Propylene Methyl Orientations for Primary and Secondary Insertions at the Metal Center

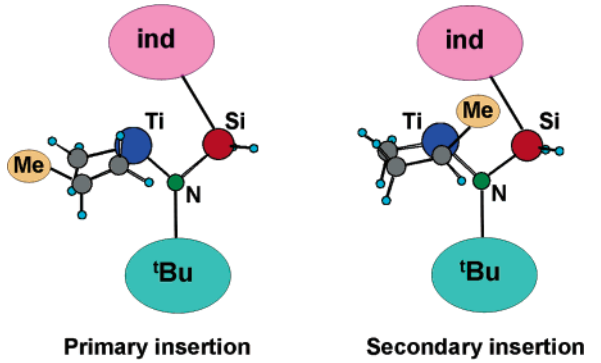

Chart 2. *Trans* and *cis* Arrangements of the Activated Propylene with Respect to the Growing Polymer Chain

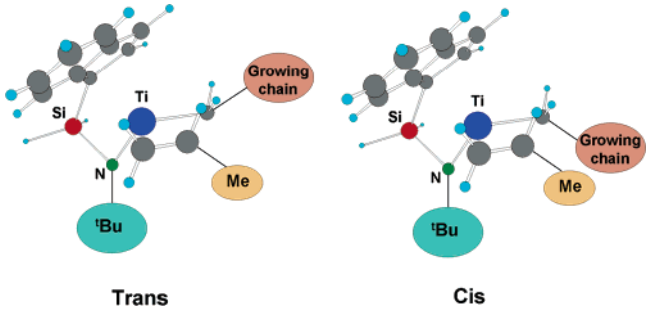

secondary insertions. Note, however, that there is no information about CGC polymerization stereoselectivity obtained from first insertions alone. In fact, for primary insertions, there are no kinetically preferred pathways as shown by the similar values of activation barriers (Figure 7), all of which lie within ~2 kcal/mol. Clearly, the propagation of the polymer chain (hence the second insertion and beyond) exerts a key influence on enchainment stereoselection, and the results of the present analysis are in excellent accord with this hypothesis.

Propylene Insertion at $H_2Si(ind)(^tBuN)Ti(^iC_4H_9)^+$ (Second Insertion). Due to the aforementioned large differences in barriers associated with primary (1,2) vs secondary (2,1) propylene insertions, only primary insertions are considered in the following analysis, and the growing polypropylene chain is pragmatically modeled as an isobutyl group. The model polymer chain introduces a new stereochemical factor. In fact, the approaching olefin methyl group may be oriented either trans or cis relative to the growing chain (Chart 2). Therefore, there are four distinct pathways for each diastereotopic catalyst site (A and B), depending on the methyl group orientation with respect to the growing chain. The four pathways are compared in Figure 8 for prototypical site A.

Activated Complexes. Relevant computed metrical data for the intermediate $H_2Si(ind)(^tBuN)Ti(^iC_4H_9)\cdots C_3H_6^+$ π-olefin complexes are summarized in Table 5. In all cases, the Ti−C(3) bond lies out of the Cp_{centr}−Ti−N plane with a 53.3°−65.8° angle, as found for the first propylene insertions. The methyl C(3)−H bond lengths and Ti−C(3)−H bond angles in the present π-olefin complexes are only slightly distorted from local C_{3v} symmetry, indicating reduced α-agostic interactions (Scheme 4). The propylene C═C π-bond vector is oriented approximately parallel or perpendicular to the Ti−C(3) bond

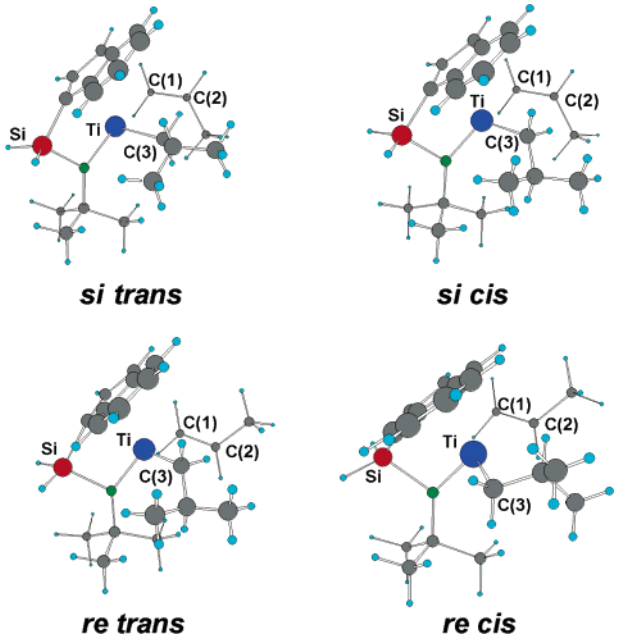

Figure 8. Second 1,2-propylene insertion pathways at $H_2Si(ind)(^tBuN)Ti(^iC_4H_9)^+$ for diastereotopic site **A** (see Figure S3 in the Supporting Information for the analogous insertions at diastereotopic site **B**).

Table 5. Selected Bond Lengths (Å), Bond and Torsion Angles (deg) of the π-Complex, Insertion Transition State, and Product for Primary Insertions of Propylene at $H_2Si(ind)(^tBuN)Ti(^iC_4H_9)^+$ (Second Insertions)[a]

	pathway A *si*		pathway A *re*		pathway B *si*		pathway B *re*	
	trans	cis	trans	cis	trans	cis	trans	cis
				π-Complex				
Ti-Cp_{centr}	2.282	2.266	2.224	2.310	2.255	2.173	2.154	2.699
Ti−N	1.862	1.864	1.866	1.863	1.861	1.879	1.878	1.832
Ti−C(1)	2.455	2.453	2.582	2.428	2.491	2.485	2.500	2.440
Ti−C(2)	2.969	2.981	3.013	2.962	3.009	3.074	3.038	2.945
Ti−C(3)	2.048	2.068	2.060	2.075	2.069	2.072	2.045	2.053
C(3)−H	1.114	1.118	1.123	1.110	1.120	1.114	1.116	1.112
Ti−C(3)−H	95.3	91.1	88.4	99.9	90.9	98.7	94.0	99.0
C(3)−Ti,C(1)−C(2)	92.2	85.1	9.2	125.6	0.0	4.4	29.7	79.6
C(3)−(N−Ti−Cp_{centr})	53.3	57.5	56.3	59.5	58.6	54.3	55.1	65.8
				Transition State				
Ti−Cp_{centr}	2.238	2.212	2.188	2.175	2.181	2.169	2.184	2.198
Ti−C(1)	2.155	2.123	2.15	2.147	2.132	2.144	2.137	2.110
Ti−C(2)	2.524	2.519	2.508	2.514	2.509	2.524	2.520	2.522
Ti−C(3)	2.172	2.203	2.167	2.145	2.185	2.149	2.173	2.206
C(3)−H	1.149	1.143	1.145	1.135	1.144	1.143	1.147	1.143
Ti−C(3)−H	62.4	61.0	62.5	65.2	62.0	62.8	61.9	60.3
C(3)−Ti,C(1)−C(2)	8.7	6.8	6.3	16.4	5.8	13.9	7.9	3.6
C(3)−(N−Ti−Cp_{centr})	37.9	44.4	43.7	39.2	41.9	38.6	41.6	45.3
				Products				
Ti−Cp_{centr}	2.132	2.142	2.153	2.148	245	2.146	2.125	2.138
Ti−C(1)	2.038	2.036	2.031	2.037	2.026	2.035	2.024	2.028
Ti−C(2)	2.778	2.665	2.657	2.642	2.656	2.657	2.716	2.640
Ti−C(3)	2.779	2.496	2.495	2.424	2.501	2.423	2.696	2.518
C(3)−H	1.135	1.123	1.125	1.115	1.123	1.117	1.133	1.128
Ti−C_α−C_β	99.8	94.4	93.9	93.0	94.0	93.9	97.2	93.5
Ti−C_α−C_β−C(3)	35.7	24.1	15.1	11.7	14.2	7.3	28.3	29.2

[a] Labeling refers to structures in Figures 8, S3 and Scheme 4.

(Table 5). In the case of both the *si trans* complex in pathway **A** and the *re trans* complex in pathway **B**, an alternative conformation is located with slightly lesser stability ($\Delta E = 2.3$−2.4 kcal/mol) and with strong agostic interactions involving the methylene group α to the Ti center.

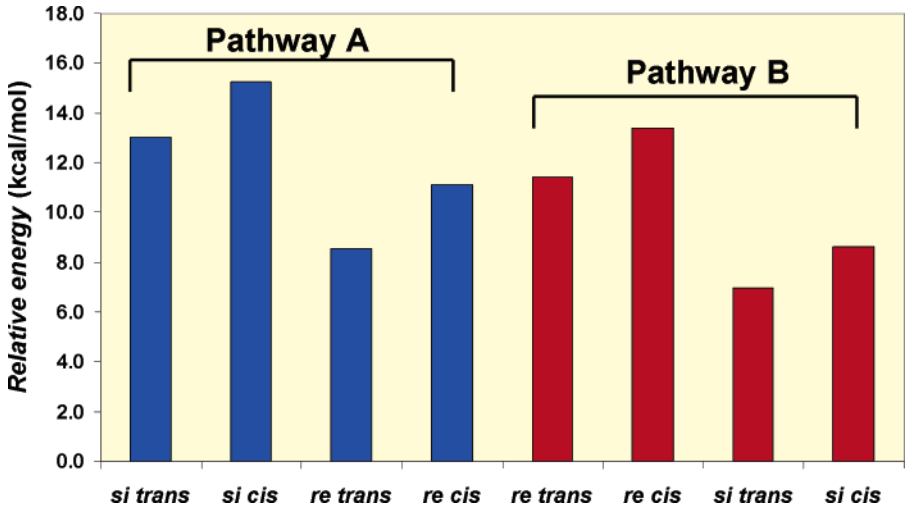

Figure 9. Energetic barriers for the second propylene insertion at $H_2Si(ind)(^tBu)Ti(^iC_4H_9)^+$ along the trajectories shown in Figures 8 and S3.

Scheme 4. Propylene Second Insertion at $H_2Si(ind)(^tBuN)Ti(^iC_4H_9)^+$ for the Primary *re trans* Pathway

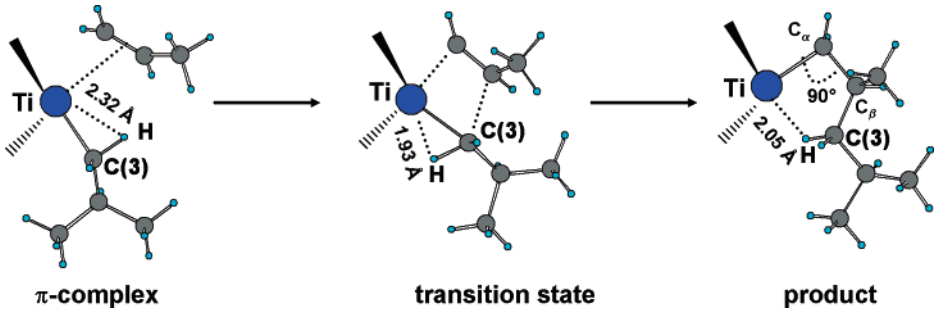

Second Insertion Transition State. The transition states associated with Ti−C propylene insertions at $H_2Si(ind)(^tBuN)Ti(^iC_4H_6)^+$ invariably involve highly distorted Ti−C(3)H_2 conformations (Table 5), compared with those of the initial π-complexes. One of the Ti−C(3)H_2 hydrogen atoms generally exhibits a strong α-agostic contact (Scheme 4). Accordingly, those C(3)−H bond lengths (Table 5) are significantly longer (∼1.14 Å) than the others (∼1.09 Å) as found for the first insertions. The geometries of the four-membered C(3)−Ti−C(1)−C(2) transition states generally exhibit small folding angles (3.6°−16.4°), with puckering arising from repulsive interactions between the methyl and propylene hydrogen atoms. These results are again in accord with those found in the first propylene insertions discussed above.

Second Insertion Product. The initial direct insertion products in all cases have γ-agostic structures with the C(3)H_2 groups (hence the C(3)−H σ bond) directed toward the vacant cationic metal coordination site (Table 5, Scheme 4). Corresponding distortions/modifications of either the Ti−C_α−C_β angle or the C(3)−H bonds are observed as a consequence of agostic interactions (Table 5). The small Ti−C_α−C_β−C(3) torsional angles (Table 5) in the γ-agostic complexes indicate near coplanarity of the three σ bonds, hence an eclipsed $C_\alpha H_2$−$C_\beta H_2$−C(3)H_2 fragment conformation.

Energetics of Second Propylene Insertions. SCF energetic data along the propylene insertion pathways at the $H_2Si(ind)(^tBuN)Ti(^iC_4H_9)^+$ naked cation are summarized in Table S3, and activation barriers are compared in Figure 9. As for ethylene insertion, **B** pathways are favored over the corresponding **A** pathways. Moreover, steric effects are, in this case, enhanced by the presence of the growing chain.

Clearly, nonbonded interactions represent the dominant contribution to the energetic differences between the various propylene insertion modes. In particular, the energy barriers depend on the spatial orientation of the propylene methyl group relative either to the growing polypropylene chain (*trans* vs *cis* conformations, Chart 2) or to the catalytic center (proximate to the *tert*-butyl group or to the asymmetric indenyl fragment, Chart 3). Thus, when the enchaining propylene methyl group and the growing chain are directed in opposite orientations (*trans* conformations), activation energies are significantly lower than those in conformations having closer contacts (*cis* conformations). Moreover, when the olefin methyl group and catalyst *tert*-butyl group are oriented in opposite directions (*re*-coordina-

Chart 3. Propylene Orientation Relative to the Catalyst *tert*-Butyl Group in Insertion Pathway **A**

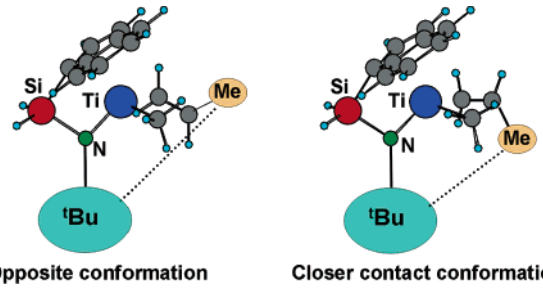

tion for pathways **A** and *si*-coordination for pathways **B**, Chart 3), the activation energies are lower than those for conformations having closer contacts (*si*-coordination for pathways **A** and *re*-coordination for pathways **B**, Chart 3).

These observations suggest that polymer propagation energetically favors pathway **B** relative to pathway **A** and, furthermore, that *si* insertions (*trans* and *cis*) are preferred in **B** pathways over *re* insertions (Figure 9) since *si* insertions have lower barriers vs all competing stereochemistries. Therefore, in a scenario of multiple insertions at the same propylene enantioface to form an isotactic microstructure (*vide supra*), the presence of these energetically preferred reaction channels (vs competing pathways) is an indication that overall $H_2Si(ind)(^t$-BuN)TiR^+ favors isospecific polypropylene enrichment, in good agreement with experiment.[30]

Conclusions

This contribution presents the first theoretical analysis of those factors governing regio- and stereochemistry associated with propylene polymerization at C_1-symmetric CGC catalysts. In particular, the present results provide considerable insight into those factors controlling reaction coordinate energetics and stereochemistry for propylene enchainment and polypropylene propagation at $H_2Si(ind)(^t$BuN)TiR^+ catalysts. In all cases, enchainment proceeds via an intermediate π-complex and subsequent insertion involving a four-center transition state. The computed thermodynamic profiles for ethylene insertion at C_1-symmetric $H_2Si(ind)(^t$BuN)$TiCH_3^+$ demonstrate unambiguously that the energetic details of such insertion processes can be analyzed in terms of SCF potential energies. SCF energy surfaces describing the ethylene insertion pathways at the H_2-Si(ind)(^{t}BuN)$TiCH_3^+$ $H_3CB(C_6F_5)_3^-$ catalyst−cocatalyst contact ion pair involve substantially higher energies because insertion requires large counteranion displacements relative to the same reaction with the parent naked cation. In particular, it is found that although electrostatic interactions within the ion pair influence catalytic activity, they have minimal impact on enchainment stereoselection for this particular catalyst, since the energetic profile associated with the π-complex, transition state, and final kinetic product progression is very similar to that of the naked catalyst cation, thus highlighting the similar stereodirecting properties of the ion pair catalyst. This result conveys a message for experimentalists in terms of cocatalyst choice.

Mechanisms associated with propylene enchainment regio- and stereochemistry have been analyzed. Data relative to the first insertions highlight the regioselectivity properties of the $H_2Si(ind)(^t$BuN)TiR^+ system. In particular, activation energies reveal that a primary (1,2) pathway is favored for the first olefin insertion, while the activation energetics for secondary (2,1) insertion are ∼5 kcal/mol greater. Data relative to the second insertions similarly reflect the stereochemical properties of the catalyst. Nonbonded repulsive effects introduced by the growing polypropylene chain, modeled here with an isobutyl group, favor preferential insertion pathways along pathway **B**, affording polymers with isotactic enrichment. In particular, the present theoretical analysis suggests that the $H_2Si(ind)(^t$BuN)TiR^+ system produces polymers with partial isotactic character, in good agreement with experiment. Clearly DFT studies can be used with confidence to predict the stereoinduction characteristics of similar single-site olefin polymerization catalysts and, hence, supply useful information for the synthesis of novel catalysts and polymers with engineered features.

Acknowledgment. This research was supported by the Ministero dell'istruzione, dell'Università e della Ricerca (MIUR Rome), the Consiglio Nazionale delle Ricerche (Rome), and by the U.S. DOE (Grant DE-FG02-86ER1351).

Supporting Information Available: Chirality elements in propylene polymerization (Figure S1 and Scheme S1). Frontside and backside olefin insertion modes (Scheme S2). First and second propylene insertion in catalyst diastereotopic site **B** (Figures S2 and S3). Energetic characterization of ethylene insertion (pathway **B**) in $H_2Si(ind)(^t$BuN)$Ti(^nC_3H_7)^+$ $H_3CB(C_6F_5)_3^-$ (Table S1). Energetic characterization of first and second propylene insertions (Table S2 and S3). A complete list of Cartesian coordinates of all structures presently analyzed. Also, complete citation of ref 25. This material is available free of charge via the Internet at http://pubs.acs.org.

JA068990X